Bending behaviors of flexible acoustic wave devices under non-uniform elasto-plastic deformation

Qian Zhang[1,2], Yong Wang[1,2,3], Dongsheng Li[1], Xin Yang[4], and Jin Xie[1,*], YongQing Fu[2,*]
Email: xiejin@zju.edu.cn; richard.fu@northumbria.ac.uk
[1]*State Key Laboratory of Fluid Power and Mechatronic Systems, Zhejiang University, Hangzhou 310027, China*
[2] *Faculty of Engineering and Environment, University of Northumbria, Newcastle upon Tyne NE1 8ST, UK*
[3]*Key Laboratory of 3D Micro/Nano Fabrication and Characterization of Zhejiang Province, School of Engineering, Westlake University, Hangzhou 310024, China*
[4]*Department of Electrical and Electronic Engineering, School of Engineering, Cardiff University, Cardiff, CF24 3AA, United Kingdom*

Flexible acoustic wave devices (FAWDs) have been explored for various applications where bending is inevitable. However, theoretical investigations of bending behavior of FAWDs hitherto are mostly done in the linear deformation regime. Herein, we develop a multi-sublayer model based on a stiffness matrix method for analysis of frequency shifts of surface acoustic wave (SAW) and Lamb waves under elasto-plastic deformations. Using this model, we calculate the frequency shifts for the cases of both an elastic bending and an elasto-plastic bending. Experimental frequency shifts of ZnO/Al flexible devices show good agreements with the theoretical results in the elastic bending tests (with a relative error of strain sensitivity < 3%), and also show relatively good agreements with the qualitative theoretical predictions in the nonlinearly elasto-plastic bending tests. For three successive bending and recovery processes, the experimentally obtained frequency shifts show good repeatability in the elastic and elasto-plastic bending stages, demonstrating maximum relative errors of strain sensitivities less than 6.1% and 18.2%.

Flexible electronics have attracted increasing attentions in recent years owing to their advantages such as portability, deformability and conformability compared to the traditionally rigid and brittle silicon-based counterparts[1-4]. Over the past decades, numerous studies on high-performance flexible electronics have been investigated, including flexible transistors[5-6], flexible energy harvesters[7], flexible resonators[8], and flexible electronic skins[9]. For realizing a good performance under a large deformation, flexible substrates including polymers[10], metallic foils[11] or inorganic thin sheets[12] are widely adopted.

SAW devices[13] have been regarded as promising for a broad range of applications such as sensing[14], acoustofluidics[15], lab-on-chip[16], and communications[17]. Recently, flexible acoustic wave devices (FAWDs) based on different substrates have been investigated, including ultra-thin glass[12] and silicon[18], $LiNbO_3$ thin film[19], polyethylene terephthalate (PET)[20], polyimide (PI)[10] and polyethylene naphthalate (PEN) films[21]. We have recently fabricated flexible SAW devices by depositing ZnO piezoelectric thin films on low-cost and commercially available aluminum (Al) thin sheets, demonstrating excellent performance for both sensing and acoustofluidics applications[22-25].

FAWDs are applied in various bending conditions, and several theoretical studies have investigated the resonant frequency shifts of flexible or rigid SAW devices under elastic strains[12, 26-27]. However, these studies generally assumed that the acoustic waves propagate in one-wavelength depth from the surface, therefore, the strain and stress distributions were assumed to be uniform. Nevertheless, these approximations are inappropriate for many SAW devices with large wavelengths (compared with the thicknesses of substrates), or for Lamb wave devices whose wavelengths are normally larger than the thicknesses of their substrates. From the bottom to the top surface of a Lamb wave device, the strains caused by a pure bending vary significantly, and a simply uniform strain approximation is inaccurate. On the other hand, owing to the good ductility of metallic Al substrate, transmission signals can be obtained even after the significant plastic deformation of the ZnO/Al device[11], which hasn't been theoretically investigated before. To theoretically analyze the frequency shift of FAWDs under elasto-plastic bending, finite element analysis (FEA) is an alternative method, whereas the complex two-dimensional

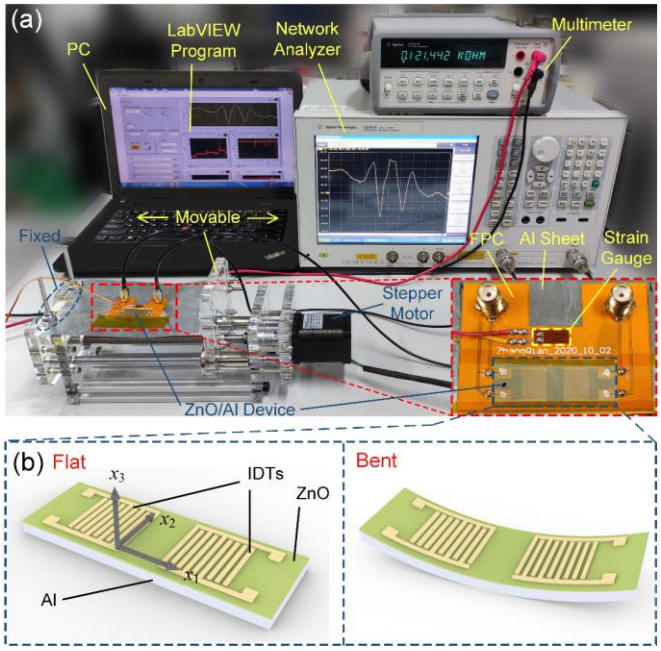

FIG. 1. (a) Experimental setup adopted for measuring the frequency responses of ZnO/Al devices under various strains. (b) Coordinate system for the calculation of the acoustic waves propagating in the ZnO/Al double layer structure as well as the flat and bent schematic drawings of the ZnO/Al device.

or three-dimensional meshes may introduce non-ignorable errors, especially when the meshes are poorly applied.

In this paper, a theoretical model was developed using a stiffness matrix method[28] and multi-sublayer approximation for the analysis of FAWDs under elasto-plastic deformations. Based on the multi-sublayer stiffness matrix method and elasto-plastic theory[29], the theoretically resonant frequency of a FAWD was solved using a MATLAB program. ZnO/Al (5 μm/50 μm thick) FAWDs with a wavelength of 64 μm and a resonant frequency of ~41.1 MHz were fabricated and the theoretical frequency shifts under the bending were calculated and compared with the experimental results. To investigate the repeatability, the frequency shifts of the ZnO/Al device under three consecutive bending and recovery processes were obtained and discussed.

ZnO/Al flexible devices were fabricated on ZnO thin film (~ 5 μm) coated Al foil (50 μm), which is flexible and easily bent. The interdigital transducers (IDTs) were patterned using the conventional photolithography and lift-off processes. As the total device thickness is ~55 μm, a wavelength larger than the device thickness (e.g., 64 μm) was adopted to generate waves propagating in the full depth. To understand the depth of acoustic wave propagating in the device, the vibration mode (A_0) was simulated using COMSOL, where a 2-dimensional piezoelectric model and a ZnO/Al (5 μm/50 μm) structure with a wavelength of 64 μm were used, as shown in Fig. S1 in the supporting information (SI). The experimental setup used for generating bending strains and measuring frequency response of ZnO/Al device is shown in Fig. 1(a). The device was taped onto a flexible printed circuit board (FPC), which was then glued onto an Al sheet. An Al sheet was fixed between two parallel polymethyl methacrylate (PMMA) boards. One of them can be moved by a stepper motor, whereas the other was fixed. Bending strain was adjusted by changing the distance between the two PMMA boards and calibrated using a strain gauge glued on the FPC. The resistance of the strain gauge was measured using a digital multimeter (Agilent 34401A). The S parameter of the ZnO/Al device (A_0 mode) was measured using a vector network analyzer (Agilent E5061B) and recorded by a LabVIEW program in real-time.

In order to investigate the acoustic waves propagating in the bent ZnO/Al device, the stiffness matrices of ZnO and Al layers were studied first. Stiffness matrix method is a numerical method used for the calculation of elastic wave propagation in a layered anisotropic media[28]. Its main idea is to calculate the stiffness matrix for each layer first, and then a recurrence relation is repeatedly used to calculate the global stiffness matrix. Combining the global stiffness matrix with the boundary conditions, the dispersion curve of the elastic wave can be solved. For the coordinate system shown in Fig. 1(b), the acoustic waves propagating in a single-layer medium without strain are governed by the constitutive Eq. (S1) in the SI. The spatial distributions of the displacement ($\boldsymbol{u}$), the electric potential ($\boldsymbol{\phi}$), the stress in the x_3 direction ($\boldsymbol{\sigma_3}$) and the electric displacement in the x_3 direction ($\boldsymbol{D_3}$) can be expressed by the following equations:

$$\boldsymbol{u} = u(x_3)\xi,\ \boldsymbol{\phi} = \phi(x_3)\xi,\ \boldsymbol{\sigma}_3 = \sigma_3(x_3)\xi,\ \boldsymbol{D}_3 = D_3(x_3)\xi \quad (1)$$

where ξ=exp[$j(\omega t-\boldsymbol{k_1}x_1)$], ω is the angular frequency, $\boldsymbol{k_1}$ denotes the wave vector in the x_1 direction, $u(x_3)$=[$u_1(x_3)$ $u_2(x_3)$ $u_3(x_3)$], $\sigma_3(x_3)$=[$\sigma_{13}(x_3)$ $\sigma_{23}(x_3)$ $\sigma_{33}(x_3)$]. By substituting (1) into Eq. (S1), we obtain the following equation[28]:

$$\left[\boldsymbol{T}(h_t)\ \boldsymbol{T}(h_b)\right]^{\mathrm{T}} = \boldsymbol{K}\left[\boldsymbol{U}(h_t)\ \boldsymbol{U}(h_b)\right]^{\mathrm{T}} \quad (2)$$

where h_t and h_b are the x_3 coordinates at the top and bottom surfaces of the layer, $\boldsymbol{U}(x_3)$=[$u(x_3)$ $\phi(x_3)$]$^{\mathrm{T}}$, $\boldsymbol{T}(x_3)$=[$\sigma_3(x_3)$ $D(x_3)$]$^{\mathrm{T}}$, and $\boldsymbol{K}$ denotes the stiffness matrix of this layer, which is an eight-order matrix determined by material properties, angular frequency and wave vector. For a layered media, the recurrence relation of $\boldsymbol{K}$ can be expressed by[24]:

$$\boldsymbol{K^N} = \begin{bmatrix} \boldsymbol{K}_{11}^{N-1} + \boldsymbol{K}_{12}^{N-1}\left(\boldsymbol{K}_{11}^{n} - \boldsymbol{K}_{22}^{N-1}\right)^{-1}\boldsymbol{K}_{21}^{N-1} & -\boldsymbol{K}_{12}^{N-1}\left(\boldsymbol{K}_{11}^{n} - \boldsymbol{K}_{22}^{N-1}\right)^{-1}\boldsymbol{K}_{12}^{n} \\ \boldsymbol{K}_{21}^{n}\left(\boldsymbol{K}_{11}^{n} - \boldsymbol{K}_{22}^{N-1}\right)^{-1}\boldsymbol{K}_{21}^{N-1} & \boldsymbol{K}_{22}^{n} - \boldsymbol{K}_{21}^{n}\left(\boldsymbol{K}_{11}^{n}\boldsymbol{K}_{22}^{N-1}\right)^{-1}\boldsymbol{K}_{12}^{n} \end{bmatrix} \quad (3)$$

where $\boldsymbol{K}^N$ is the global stiffness matrix of total N layers, $\boldsymbol{K}^{N-1} = \left[\boldsymbol{K}_{11}^{N-1}\ \boldsymbol{K}_{12}^{N-1}; \boldsymbol{K}_{21}^{N-1}\ \boldsymbol{K}_{22}^{N-1}\right]$ is the stiffness matrix of N-1 layers, $\boldsymbol{K}^{n-1} = \left[\boldsymbol{K}_{11}^{n-1}\ \boldsymbol{K}_{12}^{n-1}; \boldsymbol{K}_{21}^{n-1}\ \boldsymbol{K}_{22}^{n-1}\right]$ is the stiffness matrix of the n^{th} layer. By combining the global stiffness matrix $\boldsymbol{K}^N$ with the boundary conditions which are shown in Eq. (S5)[26], the dispersion curve can be solved. When a flexible ZnO/Al device is under a bending condition, the Eq. (S1a) should be modified into[30]:

$$\sigma_{jk}^{e}\frac{\partial^2 u_i}{\partial x_k \partial x_j} + \frac{\partial \sigma_{ji}}{\partial x_j} = \rho\frac{\partial^2 u_i}{\partial t^2} \quad (4)$$

where σ_{jk}^{e} is the external stress induced by bending, ρ is the density. According to Ref. [29], the stress distribution in the bending FAWD is a continuous function of x_3, which means $\boldsymbol{K}$ is dependent on x_3, thus resulting in the coupling between the stiffness matrix $\boldsymbol{K}$ and the state vectors ($\boldsymbol{T}$ and $\boldsymbol{U}$). In order to decouple the stiffness matrix and the state vectors to simplify the solving process, both the ZnO and Al layer are divided into multiple sublayers. Since the thickness of the sublayers is very thin (~2% of layer thickness), the strain and stress distribution in each sublayer can be assumed to be uniform, which realizes the decoupling between the stiffness matrix $\boldsymbol{K}$ and the state vectors. The strain sensitivity (SS) is defined as:

$$\mathrm{SS} = \Delta f / \Delta s \quad (5)$$

where f is resonant frequency and s is strain. For the convenience to describe the strain distributions, the nominal strain is defined as $sh/2R$, where R is the radius of curvature, h is the thickness of substrate and s is 1 for tensile strain and -1 for compressive strain.

To verify the model, COMSOL simulations were conducted for the resonant frequencies of Lamb wave devices (50 μm thick) and Rayleigh wave devices (200 μm thick) with wavelengths varied from 60 μm to 160 μm. The results show relative errors less than 2×10^{-4} when compared to those calculated using the multi-sublayer model (see D. Preliminary verification in the SI).

For the ZnO/Al (5 μm/50 μm) double layer structure, bending can be regarded as a specifically applied stress field, and the coordinate system is defined in Fig. S2(c). Density, elastic constant, strain distribution and wavelength are functions of this applied stress field, which results in the shift of the resonant

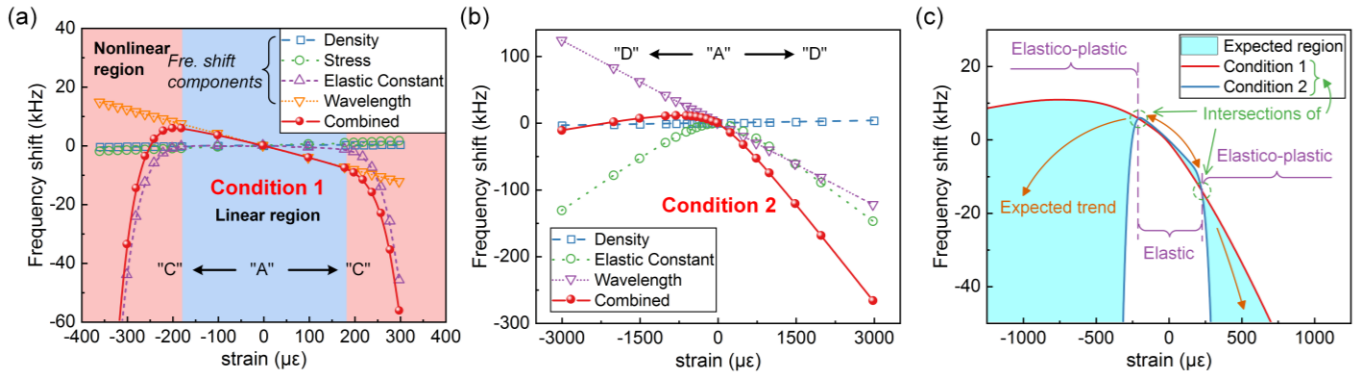

FIG. 2. Calculated total frequency shifts which are composed by frequency shift components of (a) density, stress, elastic constant and wavelength as a function of strain, with assumptions in condition 1; and (b) density, elastic constant and wavelength with assumptions in condition 2. (c) Expected region and trend of frequency shifts which are determined by the two extreme conditions (1 and 2). A ZnO/Al (5 μm/50 μm thick) device with 64 μm wavelength and parameters listed in Table. S1 are used for calculation.

frequency. For small disturbances, each of the parameter variation will contribute to frequency shift individually, and the total frequency shift can be calculated by adding these four components of frequency shift together (i.e., density, stress, elastic constant and wavelength)[26]. Due to the complexity of the elasto-plastic bending (see the detailed discussion in E. Assumptions about bending in the SI), two extreme conditions are considered. They are separated corresponding to the predicted upper and lower boundaries of the resonant frequencies of a flexible ZnO/Al device under the bending. With the points 'A', 'C' and 'D' defined in the Fig. S2(a), the first condition is in the range of 'AC', where the external stress is not released at all and the tangent modulus is defined as k_C in Fig. S2(a). The second condition is in the range of 'AD', where the external stress is fully released and the tangent modulus is described by the empirical formula as shown in Fig. S2(b). Therefore, the residual stress and the frequency shift component caused by stress are assumed to be zero in the second condition. The strain distributions of these two conditions are shown in Fig. S3.

In order to investigate the theoretical frequency shift of ZnO/Al device under the bending, a ZnO/Al (5 μm/50 μm) device with a wavelength of 64 μm was modelled in two extreme conditions with the material properties listed in the Table. S1. The A_0 mode (~41.1 MHz) was chosen in the following theoretical calculations and experiments, because its transmission signal is better than those of other modes (e.g., S_0, A_1 and S_1) in practice. The theoretical frequency shifts for the two conditions are shown in Fig. 2. For the condition 1, the total frequency shift is mainly determined by the frequency components of elastic constant and wavelength, and is approximately linear with the nominal strain in the range of -180 με to 180 με, as shown in Fig. 2(a). The frequency components of density and stress are relatively small because their distributions have opposite signs in the top and bottom half device, leading to partial cancellations between each other. The significant decrease of total frequency shift in the nonlinear region is resulted from the decrease of elastic constant caused by plastic deformation, which is also the reason for the appearance of nonlinearity. The condition 2 is similar to the first one, but the change of elastic constant is smaller, as reported in Ref. 31 and Fig. S2(b). As a result, there is no significant decrease in the total frequency shift in the second condition, as shown in Fig. 2(b). The frequency component of stress is ignored since it is assumed that no residual stress exists. By combining these two extreme conditions, the expected region of frequency shift can be obtained, as shown in Fig. 2(c). In the elastic region, the expected region is "narrow", whereas in the elasto-plastic region, it is much "wider". Therefore, we can expect that a relatively accurate theoretical result can be

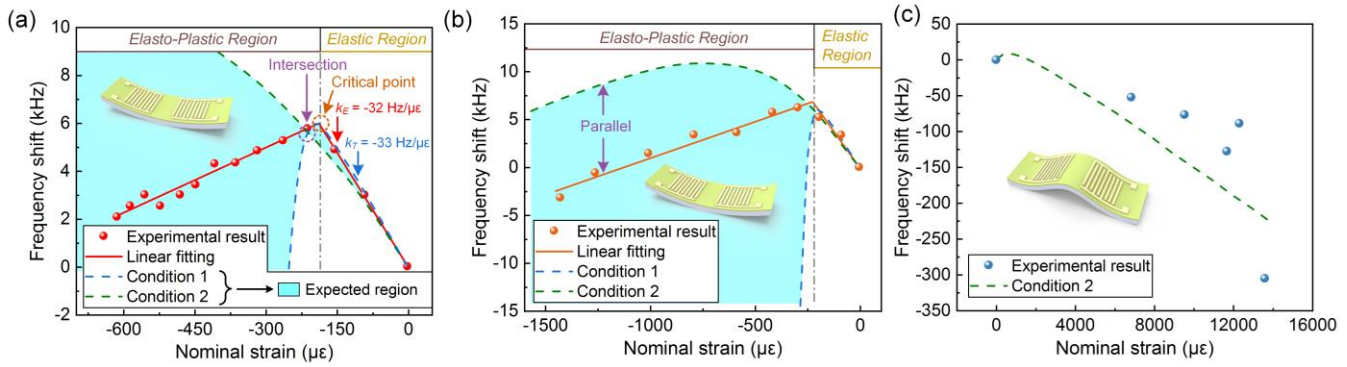

FIG. 3. Comparison of the experimental frequency shifts and the theoretical expected regions with nominal strain ranges in (a) -614 με to 0 με, (b) -1429 με to 0 με and (c) 0 με to 13629 με. The ZnO/Al (5 μm/50 μm) devices with wavelength of 64 μm are employed for both theoretical calculations and experiments, where the bending schematic drawings are shown by the corresponding insets.

obtained in the elastic region, but only rough predictions of the general trend can be obtained in the elasto-plastic region. The intersections of the curves of the two conditions where the expected region converges to points indicate the boundaries between the elastic and elasto-plastic region. As a result, the frequency-strain curve is expected to go through the two intersections.

To verify the calculated results, ZnO/Al devices with a substrate thickness of 50 μm and a wavelength of 64 μm were used in experiments. First we focus on the elastic region. As shown in Fig. 3(a), the theoretical and experimental strain sensitivities are k_T = -33 Hz/με and k_E = -32 Hz/με, respectively, which show good agreements between each other. Here the k_T is the strain sensitivity of condition 1. Then a larger strain range (-1429 με to 0 με) is considered, as shown in Fig. 3(b). In the elasto-plastic region, the shifts of experimental frequency are within the expected region with a general trend nearly parallel to the condition 2, indicating that it is possible to predict the frequency shift in a larger elasto-plastic region by simply using the condition 2. Because if the experimental frequency shift is still parallel to the condition 2 in a larger region, the difference between them is relatively small compared to the total frequency shift. Fig. 3(c) demonstrates the comparisons of theoretical (condition 2) and experimental results over a much larger range (e.g., 0 με to 13629 με). It is noteworthy that the theoretical results can correctly predict the general trend, even though the strain range is large and the frequency shift fluctuates significantly. This is probably resulted from the stress concentrations and formation of cracks which are not included in the model. Consequently, it is inferred that we can use the condition 1 for the precise calculation in the elastic region and use the condition 2 for the prediction of the general trend in the large elasto-plastic region.

The discussion above is about a single bending of the acoustic wave device. However, repeated bending and recovery are often required during the application of FAWDs. Therefore, an experiment sequence including three bending sequences (1, 2 and 3) in which the data were recorded and the recovery processes (R_1 and R_2) was further carried out in order to determine whether the theoretical model is still valid. The obtained results are shown in Fig. 4(a). The reading of the strain gauge was taken as an indicator of whether the ZnO/Al device was fully restored. For the elastic strain, Fig. 4(b) shows the similar strain sensitivities (-32 Hz/με, -31 Hz/με and -32 Hz/με) which are close to the theoretical value (-33 Hz/με), resulting in the maximum relative error of 6.1%. On the other hand, Fig. 4(c) shows the frequency shifts of device within elasto-plastic strains of -1500 με to 0 με. The measured strain sensitivities in the elastic region are -32 Hz/με, -39 Hz/με and -33 Hz/με, respectively, which are less stable but also close to the theoretical value (-33 Hz/με), resulting in the maximum relative error of 18.2%. Although the frequency shifts in elasto-plastic region for the three experiments exhibit quite large differences, their trends agree with the predicted ones. It is difficult to precisely predict the frequency shift in the elasto-plastic region owing to its complexity in deformation. To this extent, a general trend prediction rather than prediction of the exact frequency shift in the elasto-plastic region is a compromise but acceptable choice. The different elastic regions in Figs. 4(b) and 4(c) are

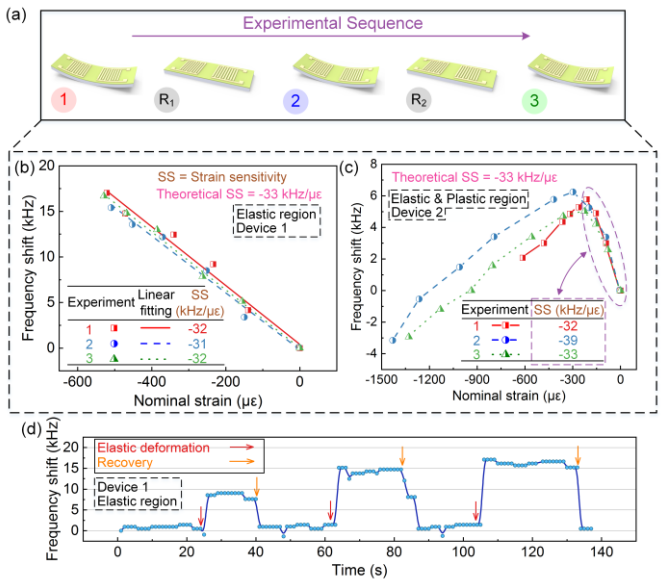

FIG. 4. Frequency shifts of ZnO/Al FAWD as a function of nominal strain in (b) elastic region and (c) elasto-plastic region, which is recorded in three consecutive experiments shown in (a). (d) Real-time frequency shifts in three consecutive bending and restoration processes. The nominal strain increase sequentially in the three bending processes but is always in elastic region.

probably caused by the pre-stress resulted from fixing. However, it has little influence on the strain sensitivity in the elastic region. Fig. 4(d) shows the real-time frequency shifts caused by strain in the elastic region. The resonant frequency is shifted when the external stress is applied, and then shifted back when the external stress is removed, demonstrating a good repeatability. In summary, the theoretical model is valid for the predictions of resonant frequencies of FAWDs under repeated elasto-plastic bending and recovery processes, without considering fatigue and defect generations in the materials.

In this work, the multi-sublayer stiffness matrix method was developed for the design and calculation of flexible harmonic acoustic wave device under the non-uniform elasto-plastic deformation. The calculated resonant frequencies using the multi-sublayer model were compared with the simulation results of COMSOL when no strain was applied, showing good consistency that the relative errors were less than 2×10^{-4}. The theoretical frequency shift region was calculated and discussed based on the two extreme strain conditions. Experimental results were compared with the theoretical expectations, demonstrating quantitative predictions in the elastic region (relative error of strain sensitivity < 3%) and well predictions of trends in the elasto-plastic region. Finally, the bending repeatability of the ZnO/Al device was investigated by the consecutive bending and recovery processes, and the experimental frequency shifts were within the predicted data region. The relative errors of strain sensitivity in the elastic region were less than 6.1% for pure elastic bending and 18.2% for elasto-plastic bending.

SUPPLEMENTARY MATERIAL

Detailed assumptions and discussions about elasto-plastic bending, preliminary verification for the multi-sublayer model,

and parameters used for the calculations can be found in the supplementary material.

ACKNOWLEDGEMENTS

This work was supported by the "National Natural Science Foundation of China (51875521)", the "Zhejiang Provincial Natural Science Foundation of China (LZ19E050002)", the UK Engineering and Physical Sciences Research Council (EPSRC EP/P018998/1 and UK Fluidic Network (EP/N032861/1)-Special Interest Group in Acoustofluidics), and Newton Mobility Grant (IE161019) through Royal Society and NFSC.

DATA AVAILABILITY

The data that support the findings of this study are available within the article and its supplementary material.

[1] H. Yang, W.R. Leow, and X. Chen, Small Methods **2**, 1 (2018).
[2] J.L. Wang, M. Hassan, J.W. Liu, and S.H. Yu, Adv. Mater. **30**, 1 (2018).
[3] J. Chen, J. Liu, T. Thundat, and H. Zeng, ACS Appl. Mater. Interfaces **11**, 18720 (2019).
[4] Y. Wan, Z. Qiu, J. Huang, J. Yang, Q. Wang, P. Lu, J. Yang, J. Zhang, S. Huang, Z. Wu, and C.F. Guo, Small **14**, 1 (2018).
[5] K. Myny, Nat. Electron. **1**, 30 (2018).
[6] J. Kwon, Y. Takeda, R. Shiwaku, S. Tokito, K. Cho, and S. Jung, Nat. Commun. **10**, 1 (2019).
[7] D.H. Kim, H.J. Shin, H. Lee, C.K. Jeong, H. Park, G.T. Hwang, H.Y. Lee, D.J. Joe, J.H. Han, S.H. Lee, J. Kim, B. Joung, and K.J. Lee, Adv. Funct. Mater. **27**, 1 (2017).
[8] L. Zhang, C. Gao, Y. Jiang, B. Liu, M. Zhang, H. Zhang, Q. Li, X. Chen, and W. Pang, Adv. Electron. Mater. **5**, 1 (2019).
[9] G. Schwartz, B.C.K. Tee, J. Mei, A.L. Appleton, D.H. Kim, H. Wang, and Z. Bao, Nat. Commun. **4**, (2013).
[10] W. Xuan, X. He, J. Chen, W. Wang, X. Wang, Y. Xu, Z. Xu, Y.Q. Fu, and J.K. Luo, Nanoscale **7**, 7430 (2015).
[11] Y. Liu, Y. Li, A.M. El-Hady, C. Zhao, J.F. Du, Y. Liu, and Y.Q. Fu, Sensors Actuators, B Chem. **221**, 230 (2015).
[12] J. Chen, H. Guo, X. He, W. Wang, W. Xuan, H. Jin, S. Dong, X. Wang, Y. Xu, S. Lin, S. Garner, and J. Luo, J. Micromechanics Microengineering **25**, (2015).
[13] Y.Q. Fu, J.K. Luo, N.T. Nguyen, A.J. Walton, A.J. Flewitt, X.T. Zu, Y. Li, G. McHale, A. Matthews, E. Iborra, H. Du, and W.I. Milne, Prog. Mater. Sci. **89**, 31 (2017).
[14] K. Chang, Y. Pi, W. Lu, F. Wang, F. Pan, F. Li, S. Jia, J. Shi, S. Deng, and M. Chen, Biosens. Bioelectron. **60**, 318 (2014).
[15] F. Guo, Z. Mao, Y. Chen, Z. Xie, J.P. Lata, P. Li, L. Ren, J. Liu, J. Yang, M. Dao, S. Suresh, and T.J. Huang, Proc. Natl. Acad. Sci. U. S. A. **113**, 1522 (2016).
[16] S. Li, X. Ding, F. Guo, Y. Chen, M.I. Lapsley, S.C.S. Lin, L. Wang, J.P. McCoy, C.E. Cameron, and T.J. Huang, Anal. Chem. **85**, 5468 (2013).
[17] X. Lu, K. Mouthaan, and Y.T. Soon, IEEE Trans. Microw. Theory Tech. **62**, 28 (2014).
[18] C.H. Zhang, Y. Yang, C.J. Zhou, Y. Shu, H. Tian, Z. Wang, Q.T. Xue, and T.L. Ren, Chinese Phys. Lett. **30**, (2013).
[19] H. Xu, S. Dong, W. Xuan, U. Farooq, S. Huang, M. Li, T. Wu, H. Jin, X. Wang, and J. Luo, Appl. Phys. Lett. **112**, (2018).
[20] X. He, H. Guo, J. Chen, W. Wang, W. Xuan, Y. Xu, and J. Luo, Appl. Phys. Lett. **104**, 1 (2014).
[21] L. Lamanna, F. Rizzi, V.R. Bhethanabotla, and M. De Vittorio, Biosens. Bioelectron. **163**, 112164 (2020).
[22] R. Tao, W.B. Wang, J.T. Luo, S. Ahmad Hasan, H. Torun, P. Canyelles-Pericas, J. Zhou, W.P. Xuan, M.D. Cooke, D. Gibson, Q. Wu, W.P. Ng, J.K. Luo, and Y.Q. Fu, Surf. Coatings Technol. **357**, 587 (2019).
[23] R. Tao, G. Mchale, J. Reboud, J.M. Cooper, H. Torun, J.T. Luo, J. Luo, X. Yang, J. Zhou, P. Canyelles-Pericas, Q. Wu, and Y. Fu, Nano Lett. **20**, 3263 (2020).
[24] X. Tao, H. Jin, M. Mintken, N. Wolff, Y. Wang, R. Tao, Y. Li, H. Torun, J. Xie, J. Luo, J. Zhou, Q. Wu, S. Dong, J. Luo, L. Kienle, R. Adelung, Y.K. Mishra, and Y.Q. Fu, ACS Appl. Nano Mater. **3**, 1468 (2020).
[25] R. Tao, J. Reboud, H. Torun, G. McHale, L.E. Dodd, Q. Wu, K. Tao, X. Yang, J.T. Luo, S. Todryk, and Y. Fu, Lab Chip **20**, 1002 (2020).
[26] H. Xu, Z. Cao, S. Dong, J. Chen, W. Xuan, W. Cheng, S. Huang, L. Shi, S. Liu, U. Farooq, A. Qadir, and J. Luo, J. Micromechanics Microengineering **29**, (2019).
[27] B. Donohoe, B. Mc Cormack, D. Geraghty, and G.E. O'Donnell, Proc. IEEE Sensors 1665 (2011).
[28] S.I. Rokhlin and L. Wang, J. Acoust. Soc. Am. **112**, 822 (2002).
[29] J. Lubliner, *Plasticity Theory*. 229-249 (Courier Corporation, 2008).
[30] A.L. Nalamwar and M. Epstein, J. Appl. Phys. **47**, 43 (1976).
[31] Q.G. Wang, Metall. Mater. Trans. A Phys. Metall. Mater. Sci. **35 A**, 2707 (2004).